ADVANCED MATERIALS

Supporting Information

for *Adv. Mater.*, DOI: 10.1002/adma.202002297

Boosting Neutral Water Oxidation through Surface Oxygen Modulation

Longsheng Zhang, Liping Wang, Yunzhou Wen, Fenglou Ni, Bo Zhang, and Huisheng Peng**

Supporting Information for

Boosting neutral water oxidation through surface oxygen modulation

This file includes:

Materials and Methods.

Figure S1 to S17.

Table S1 to S4.

Reference List.

Materials and Methods

Chemicals

Ruthenium chloride hydrate ($RuCl_3 \cdot xH_2O$), calcium chloride dehydrate ($CaCl_2 \cdot 2H_2O$) and sodium hexachloroiridate hydrate ($Na_3IrCl_6 \cdot xH_2O$), propylene oxide (≥99%), Nafion® (5 wt% in mixture of lower aliphatic alcohols and water), ruthenium oxide (RuO_2) and Iridium oxide (IrO_2) were purchased from Sigma-Aldrich. Ethanol, isopropanol, acetone and N, N-dimethylformamide (DMF) were purchased from Sinopharm Chemical Reagent Co., Ltd. Carbon black (20 nm) was purchased from Suzhou Tanfeng Co., Ltd. All chemicals were used without any further purification.

Synthesis of catalysts

$RuIrCaO_x$ and $RuIrO_x$ catalysts were synthesized *via* a modified sol-gel technique.[1] $RuCl_3 \cdot xH_2O$ (0.3 mmol), $CaCl_2 \cdot 2H_2O$ (0.2 mmol) and $Na_3IrCl_6 \cdot xH_2O$ (0.1 mmol) were first dissolved in DMF (4 mL) in a vial. Then the solution was sealed and cooled in a refrigerator for 2 h in order to prevent uncontrolled hydrolysis. Propylene oxide (0.5 mL) was slowly dropwise added under stirring. The solution was aged for 1 day and black precipitates would appear. Afterwards, the solution and precipitates were transferred into a vial and immersed in acetone for 3 days, before the precipitates were collected *via* centrifugation and washed by acetone for 5 times to thoroughly remove DMF and propylene oxide. The precipitates were dried in vacuum and then grinded carefully. Finally, the as-obtained black powder was placed into a tube furnace and annealed at 400 ^oC in air for 2 h to obtain $RuIrCaO_x$ catalyst. Accordingly, $RuIrO_x$ catalyst was also synthesized using a similar procedure without $CaCl_2 \cdot 2H_2O$.

Characterization

Transmission electron microscopy (TEM) and energy-dispersive spectroscopy (EDS) were performed with a JEOL JEM-2100 TEM at an acceleration voltage of 200 kV. The $RuIrCaO_x$ catalysts were subjected to oxygen evolution reaction (OER) before TEM observation. The TEM samples were prepared by dropping catalysts dispersed in ethanol onto carbon-coated copper grids, and were dried in vacuum for 6 h. X-ray

diffraction (XRD) patterns were collected from a MiniFlex600 X-ray diffractometer with Cu K_α radiation (λ = 0.1542 nm) under a voltage of 40 kV and a current of 40 mA. The molar ratios of metal elements for $RuIrCaO_x$ and $RuIrO_x$ samples were quantified by inductively coupled plasma-mass spectrometry (ICP-MS, iCAP7400, Thermo Fisher). Thermogravimetry (TG) measurements (Pyris 1, PerkinElmer) were carried out under air flow from 35 to 200 ℃ with a heating rate of 10 ℃/min. Mass specific surface areas of the catalysts were determined *via* Brunauer, Emmett, and Teller (BET) area measurements. N_2 adsorption-desorption isotherms of the catalysts were measured at -196 ℃ using a Quantachrome QUADRASORB SI analyzer. X-ray photoelectron spectroscopy (XPS) spectra were obtained from a VG ESCALAB 220I-XL device. All XPS spectra were corrected using C1s line at 284.8 eV. The curve fitting of all XPS spectra was accomplished using XPS Peak 4.1 software.

X-ray absorption fine spectroscopy (XAFS) measurements

The *in-situ* Ru K-edge and Ir L_3-edge measurements were carried out at 1W1B beamline in Beijing Synchrotron Radiation Facility (BSRF). A home-made triangular electrochemical cell was used, which was equipped with three-electrode configuration. The electrochemical cell was placed in the middle of the optical path with an incident angle of 45^o. The working electrodes were prepared by spray coating the catalysts on carbon paper. For the *in-situ* XAFS measurements, potentiostatic reaction at 1.55 V (*vs.* reversible hydrogen electrode, RHE) were employed and fluorescent mode was used to acquire XAFS data. The energy of Ru K-edge was calibrated by Ru foil and the energy of Ir L_3-edge was calibrated by Pt foil. All XAFS data were processed and normalized by ATHENA software included in IFEFFIT software package.

Soft X-ray absorption spectroscopy (sXAS) measurements

The *quasi in-situ* sXAS measurements of O *K*-edges were performed at the Spherical Grating Monochromator (SGM) beamline of Canadian Light Source (CLS). The scanning energy ranges of O *K*-edges were set between 525 and 564 eV. The *quasi in-situ* sXAS measurements of Ca *L*-edges were performed at beamline 4B9B of

Beijing Synchrotron Radiation Facility (BSRF). The scanning energy ranges of Ca *L*-edges were set between 330 and 360 eV. The spectra of O *K*-edges and Ca *L*-edges were collected in total electron yield mode in an ultrahigh-vacuum chamber.

Differential electrochemical mass spectrometry (DEMS) measurements

DEMS measurements were carried out to determine the ^{18}O-labeled volatile reaction products of $RuIrCaO_x$ and $RuIrO_x$ catalysts during OER process using a QAS 100 device (Linglu Instruments, Shanghai). First, the catalysts were dispersed on gold disk electrodes (3 mm in diameter) with a same loading mass (0.65 mg/cm^2), and then labeled with ^{18}O isotopes by being oxidized for 10 min in ^{18}O-labeled 0.5 M $KHCO_3$ aqueous electrolyte at 1.6 V (*vs.* gold counter electrode). Afterwards, electrodes were rinsed with ^{16}O water five times to remove $H_2{}^{18}O$ and scanned in 0.5 M $KHCO_3$ solution of $H_2{}^{16}O$ from 0.67 to 1.07 V (*vs.* Ag/AgCl) at a rate of 2 mV/s. Gas products of different molecular weights generated during OER process were measured in real time by mass spectroscopy. Because catalyst electrodes were rinsed with ^{16}O water after ^{18}O-labelling, it is unlikely that ^{18}O species adsorbed on the surface contribute substantially to the observed $^{34}O_2$ ($^{16}O^{18}O$) signals. Thus, it can be determined to investigate the participation of lattice oxygen from catalysts in OER by measuring the $^{34}O_2$ signals (see Figure 4a).

Secondary ion mass spectroscopy (SIMS) measurements

SIMS experiments were performed to determine the ^{18}O and ^{16}O isotopes in catalysts using a TOF.SIMS 5 device (ION-TOF GmbH). First, $RuIrCaO_x$ and $RuIrO_x$ catalysts were dispersed on carbon-paper electrodes, and then held for galvanostatic reaction for 6 h in ^{18}O-labeled 0.5 M $KHCO_3$ aqueous electrolyte. After rinsed with ^{16}O water, the catalyst electrodes were finally heated at 150 ℃ in vacuum for 6 h to remove adsorbed $H_2{}^{18}O$. By measuring the $^{18}O/^{16}O$ intensity ratio at the surface of catalysts, the frequencies of lattice-oxygen exchange can be determined. The $^{18}O/^{16}O$ intensity ratio of $RuIrCaO_x$ catalyst is about 67%, which is greatly higher than that (4%) of $RuIrO_x$ catalyst (see Figure 4c).

Electrochemical measurements

Electrochemical measurements were conducted using a three-electrode configuration connected to an electrochemical workstation (MULTI Autolab M204). Ag/AgCl (with 3.5 M KCl as the filling solution) and platinum foil were used as reference and counter electrodes, respectively.

Typically, 10 mg of catalysts and 2 mg carbon black were dispersed in a 1.25 mL mixture of water and ethanol (4/1, v/v), and then 80 μL of Nafion® solution (5 wt%) was added. The suspension was immersed in an ultrasonic bath for 40 min to prepare a homogeneous ink. Then, working electrode was prepared by depositing 4 μL of the catalyst ink onto glassy carbon electrodes (GCEs, 3 mm in diameter).

To load the catalysts on gold foam (thickness: 1.6 mm), 20 mg of catalyst powders was dispersed in a 4 mL mixture of water and ethanol (1/1, v/v), followed by the addition of 100 μL Nafion® solution. The suspension was sonicated for 40 min to prepare a homogeneous ink. The gold foam with a fixed area of 0.5 × 0.5 cm^2 coated with water resistant silicone glue was drop-casted with 400 μL of the catalyst ink.

To assess the OER catalytic activity, the working electrode was first scanned from 0.6 to 0.9 V (*vs.* Ag/AgCl) at a rate of 50 mV/s for 20 cycles to achieve stable cyclic voltammetry (CV) scans in CO_2-saturated 0.5 M $KHCO_3$ aqueous electrolyte. Then linear sweep voltammetry (LSV) with a scan rate of 5 mV/s were measured. Unless otherwise stated, all CV and LSV measurements were conducted at room temperature (23±2 ^oC). All potentials were referred to reversible hydrogen electrode (RHE) by Equation 1:

$$E_{RHE} = E_{Ag/AgCl} + 0.2046 + 0.059 \times pH \quad (1)$$

The galvanostatic measurement with $RuIrCaO_x$ catalyst loaded onto gold foam electrode was conducted at a constant current density of 10 mA/cm^2 (currents are normalized to projected geometric area). During the galvanostatic measurement, a

flow of CO_2 gas (99.99% purity) into the electrolyte was maintained during the test. The electrochemical cell was placed in a 25±2 ^{o}C thermostatic waterbath.

Electrochemical active surface area (ECSA) calculation

The ECSA of catalysts were calculated based on their electrical double layer capacitor (C_{dl}), which were obtained from CV plots in a narrow non-Faradaic potential window from 0.175 to 0.275 V (*vs.* Ag/AgCl). The anodic currents at 0.225 V (*vs.* Ag/AgCl) were plotted as a function of scan rate. Then linear fitting was adopted to these points, and the slope of plots gives the value of C_{dl}. The specific capacitance was found to be 35 μF/cm^2,[2] and the ECSA values of catalysts were calculated from Equation 2:

$$ECSA = \frac{C_{dl}}{35\ \mu F/cm^2} cm^2_{ECSA} \quad (2)$$

The specific activity was revealed by normalizing the current to the ECSA to exclude the effect of surface area on catalytic performance. The ECSA values and specific activities of catalysts are listed at Table S3.

Turnover frequencies (TOFs) calculation

The TOF values of catalysts on GCEs were calculated from Equation 3:

$$TOF = \frac{j \times A}{4 \times F \times n} \quad (3)$$

where *j* is the current density obtained at 1.63 V (*vs.* RHE), A is the geometric area, F is the Faraday constant and n is the mole number of active metal atoms on GCE *via* Equation 4:

$$n = \frac{m_{loading}}{Mw} \times r \quad (4)$$

where $m_{loading}$ is the loading mass of catalyst on GCE, r is the molar ratio of all metal atoms in catalyst and Mw is the molecular weight of catalyst. In this work, the molar ratios of Ru/Ir/Ca elements are 0.49/0.24/0.43 for $RuIrCaO_x$ sample and the molar ratio of Ru/Ir elements is 0.50/0.21 for $RuIrO_x$ sample according to the results from ICP-MS analysis (Table S1). The TOF values of $RuIrCaO_x$ and $RuIrO_x$ catalysts were calculated according to the mass loading of active metal atoms (both Ru and Ir), which were listed at Table S3.

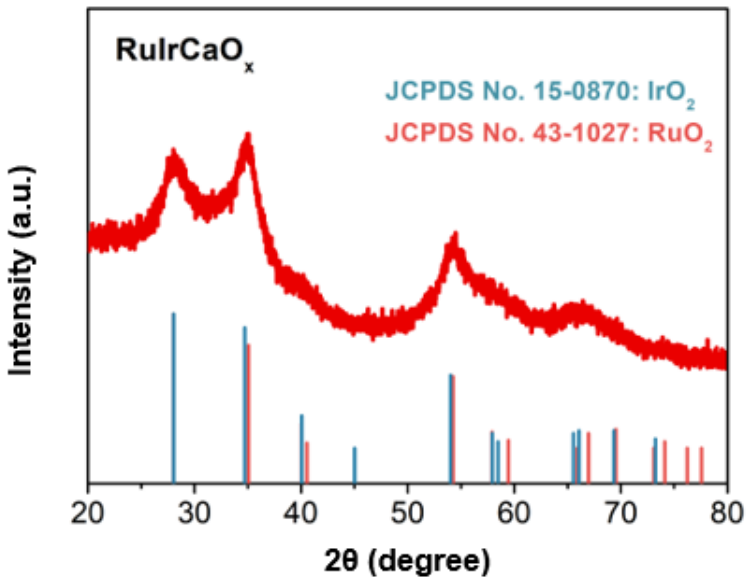

Figure S1. XRD pattern of $RuIrCaO_x$ sample.

The XRD peaks of $RuIrCaO_x$ sample are in accordance with those of IrO_2 (JCPDS card No. 15-0870) and RuO_2 (JCPDS card No. 43-1027). No impurity phases are shown in the XRD pattern of $RuIrCaO_x$ sample.

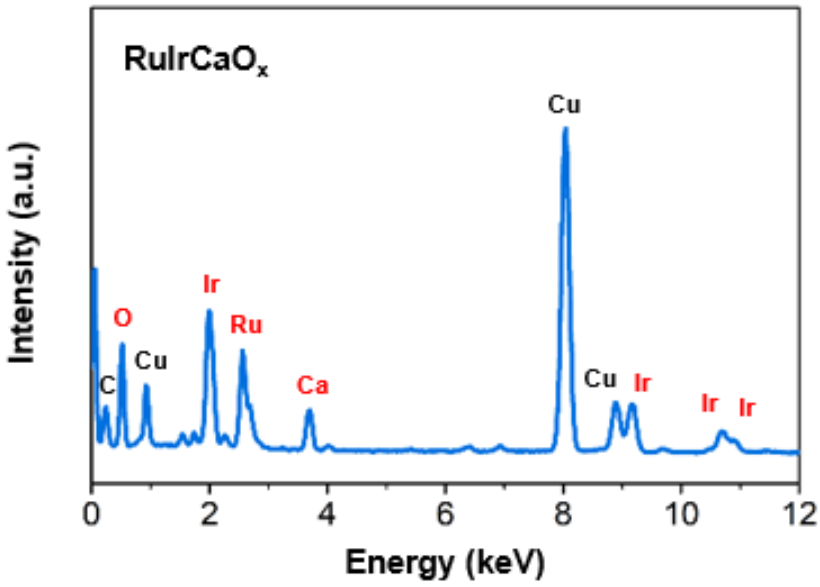

Figure S2. EDS spectrum of $RuIrCaO_x$ sample.

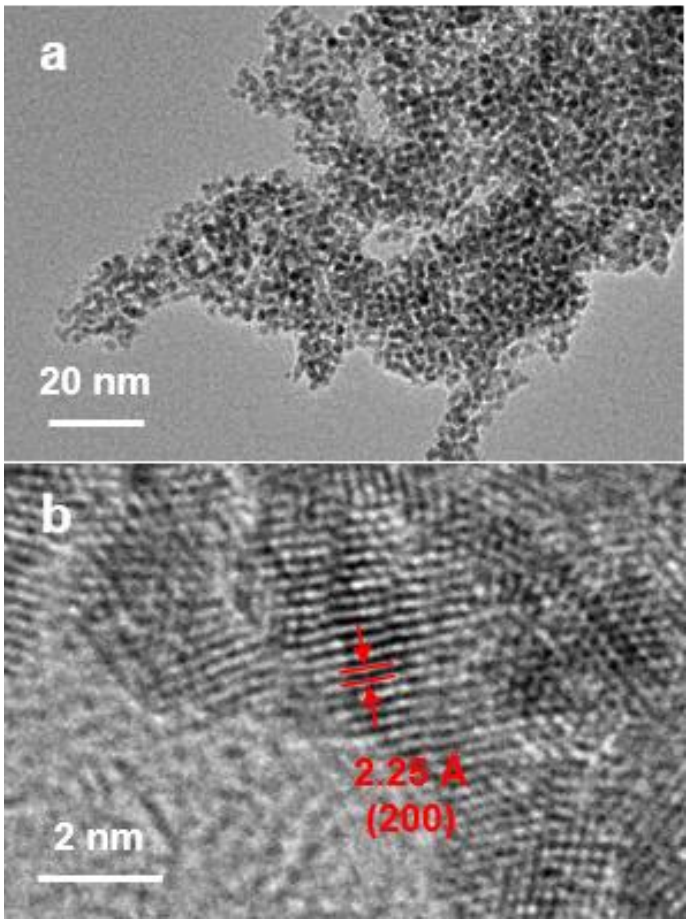

Figure S3. (a, b) TEM images of $RuIrCaO_x$ sample.

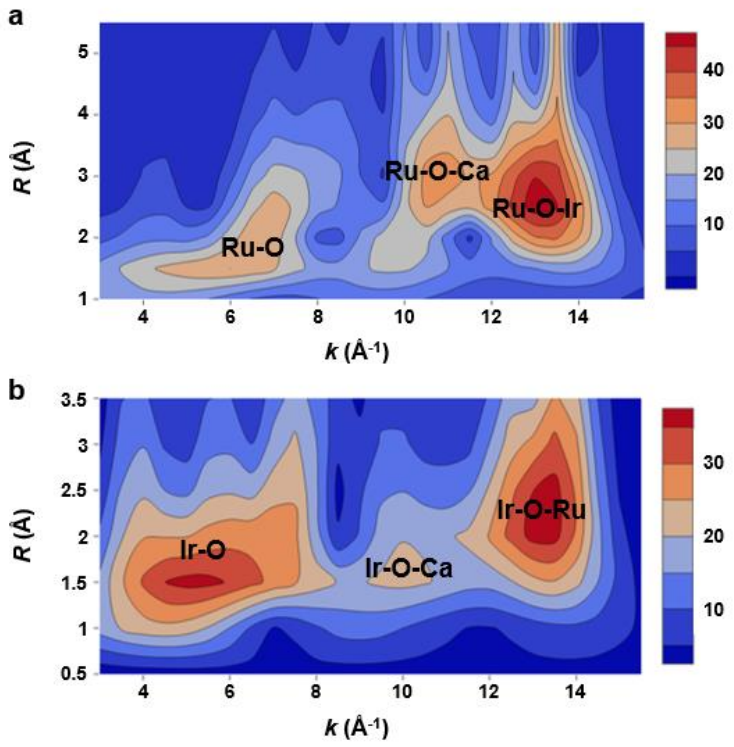

Figure S4. The Morlet Wavelet transformation map of **(a)** Ru K-edge and **(b)** Ir L_3-edge extended X-ray absorption fine structure (EXAFS) spectra.

As shown in Figure S4, the Morlet wavelet transformation of EXAFS results reveal significant peaks of Ru-O-Ca/Ir-O-Ca in $RuIrCaO_x$ catalyst, indicating the formation of Ru-O-Ca and Ir-O-Ca bonds in $RuIrCaO_x$ catalyst.

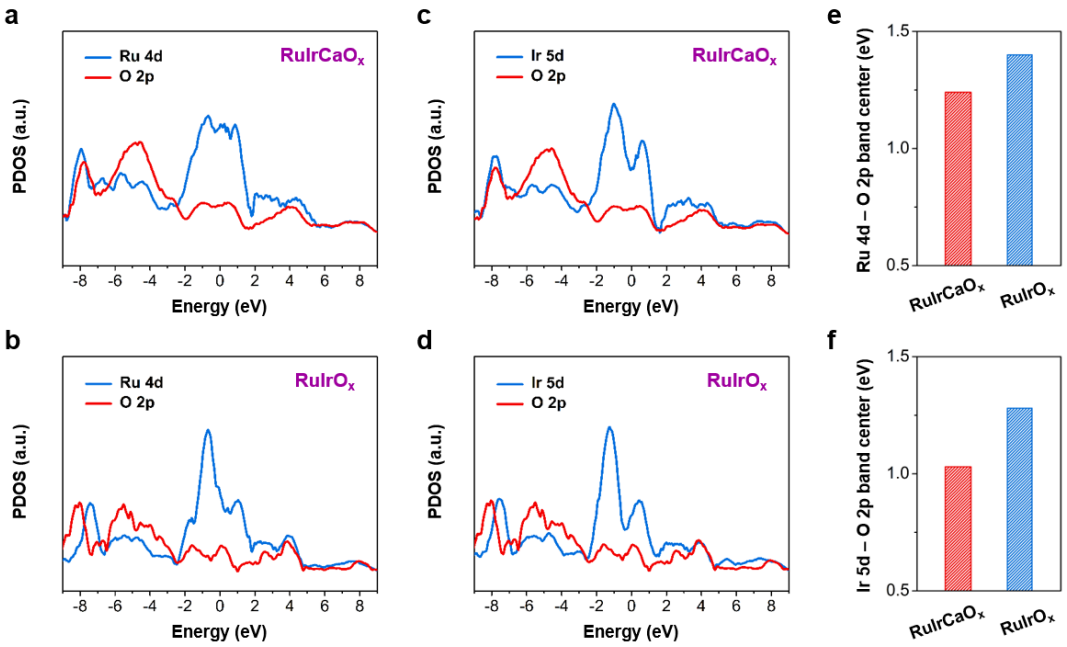

Figure S5. (a, b) Projected densities of states of Ru 4*d* and oxygen 2*p* states for $RuIrCaO_x$ and $RuIrO_x$, respectively. **(c, d)** Projected densities of states of Ir 5*d* and oxygen 2*p* states for $RuIrCaO_x$ and $RuIrO_x$, respectively. **(e, f)** Difference between the metal *d* and O *2p*-band center, respectively.

As shown in Figure S5, after incorporating Ca^{2+}, the difference between metal *d* (Ru *4d* and Ir *5d*) and oxygen 2*p*-band center are both smaller, indicating the enhanced metal-oxygen hybridization between metal *d* and oxygen 2*p* states.

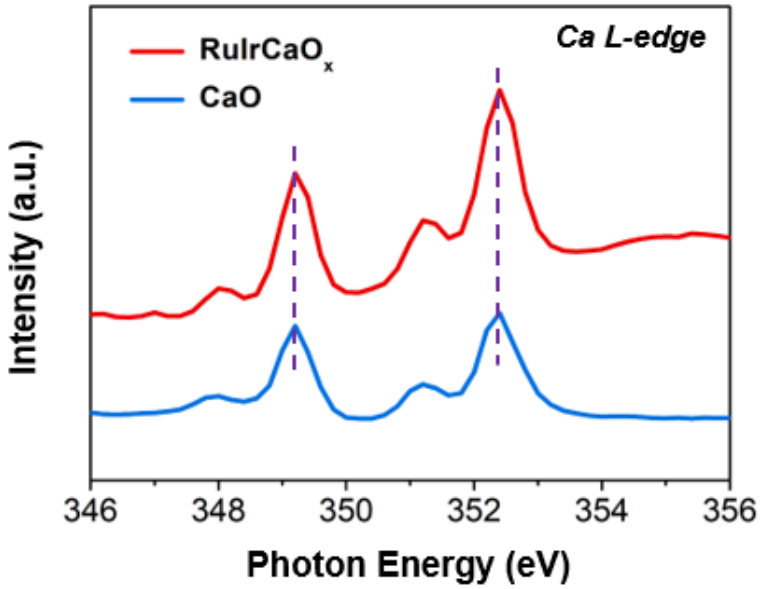

Figure S6. Ca L-edge sXAS spectra of $RuIrCaO_x$ sample and CaO reference.

The peaks observed in the Ca L-edge sXAS spectrum of $RuIrCaO_x$ sample are similar to those of CaO reference, indicating Ca^{2+} is dominant oxidation state in $RuIrCaO_x$ sample.

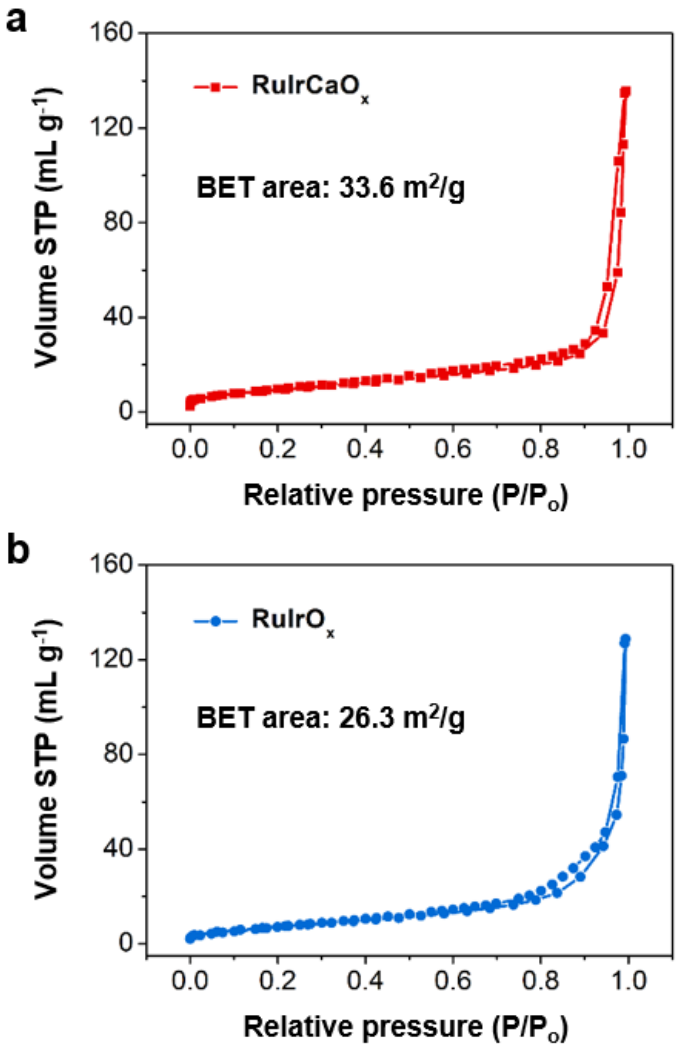

Figure S7. (a, b) BET isotherms of $RuIrCaO_x$ and $RuIrO_x$ samples, respectively.

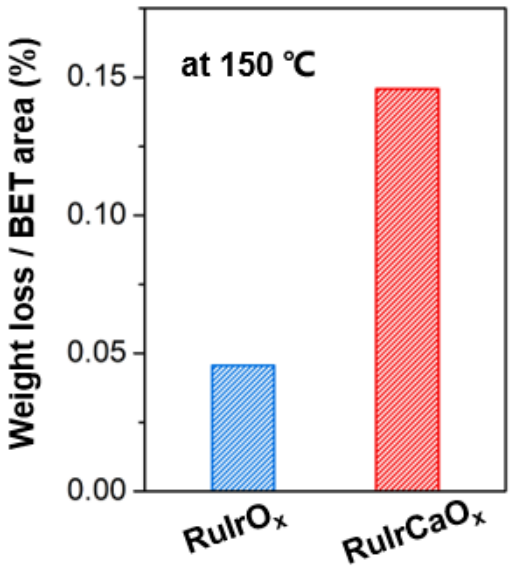

Figure S8. The percentage of TG weight loss at 150 ℃ for $RuIrO_x$ and $RuIrCaO_x$ samples, normalized by their BET specific surface area.

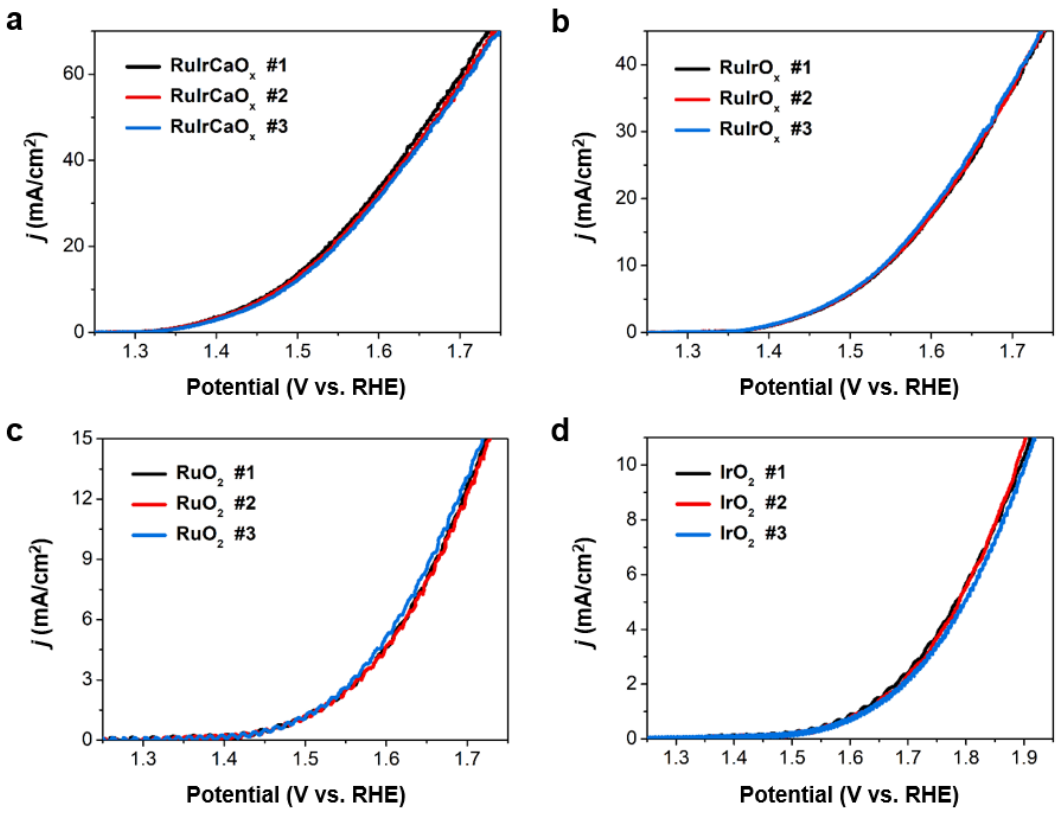

Figure S9. (a-d) Three independent LSV tests for $RuIrCaO_x$, $RuIrO_x$, benchmark RuO_2 and IrO_2 catalysts on GCEs measured at a scan rate of 5 mV/s in CO_2-saturated 0.5 M $KHCO_3$ aqueous electrolyte, respectively.

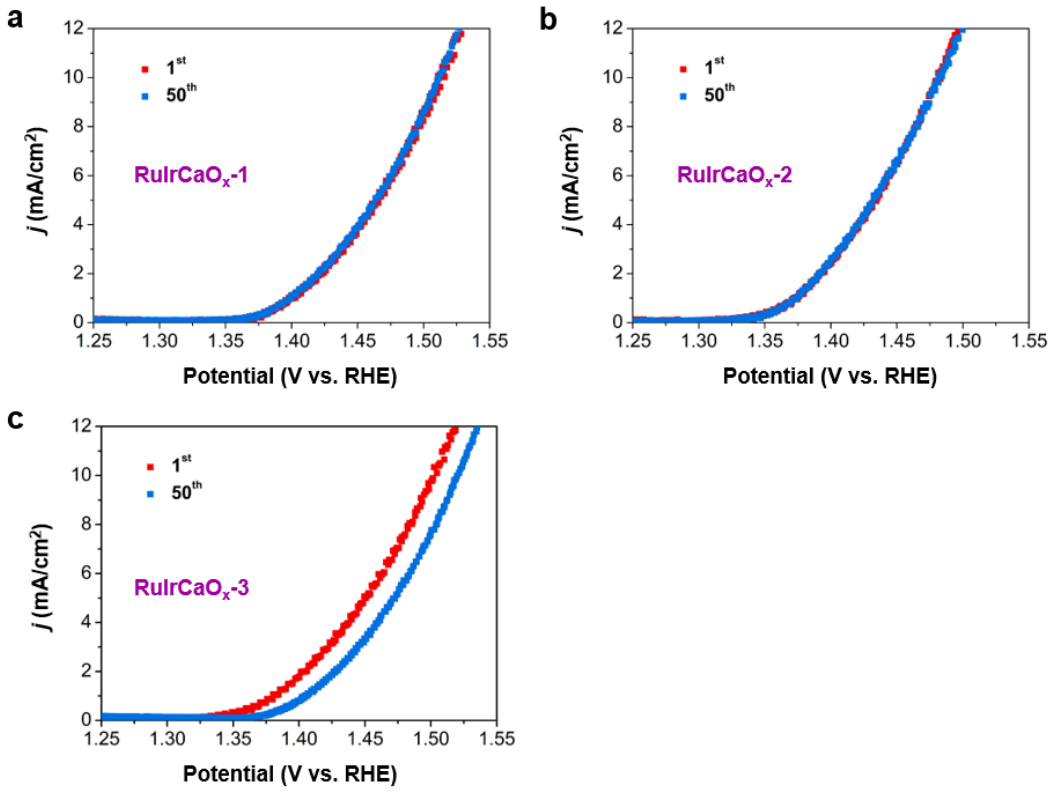

Figure S10. LSV curves of $RuIrCaO_x$ catalysts with different contents of Ca^{2+} on GCEs at a scan rate of 5 mV/s in CO_2-saturated 0.5 M $KHCO_3$ aqueous electrolyte.

$RuIrCaO_x$ catalysts with increasing contents of Ca^{2+} were synthesized by adjusting the feed ratios of Ru/Ir/Ca salt precursors (3/1/1, 3/1/2, 3/1/3), which were denoted as $RuIrCaO_x$-1, $RuIrCaO_x$-2 and $RuIrCaO_x$-3, respectively. As shown in Figure S10, the $RuIrCaO_x$-1 catalyst with lowest content of Ca^{2+} exhibited lowest catalytic activity. The $RuIrCaO_x$-3 catalyst with highest content of Ca^{2+} exhibited highest catalytic activity but poor stability. Among these catalysts, the $RuIrCaO_x$-2 catalyst exhibited optimal OER performance combining the activity and stability.

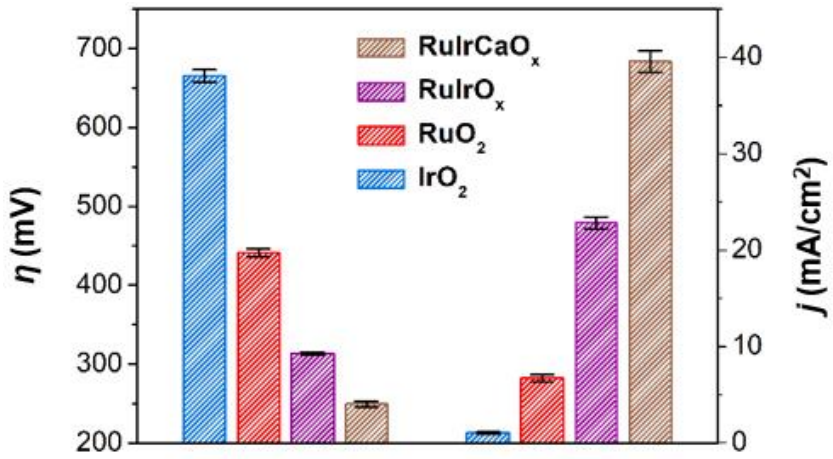

Figure S11. Comparison of overpotential (η) at 10 mA/cm^2 (left axis) and current density (j) at 1.63 V *vs*. RHE (right axis) for different catalysts on GCEs.

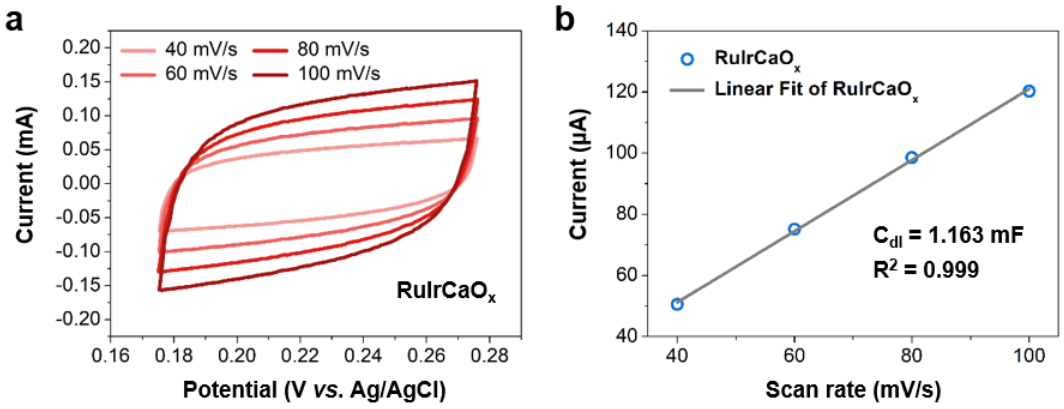

Figure S12. (a) CV curves recorded at different scan rates for $RuIrCaO_x$ catalyst in a non-Faradaic potential window from 0.175 to 0.275 V (vs. Ag/AgCl). **(b)** Current as a function of scan rate to give the C_{dl} for $RuIrCaO_x$ catalyst.

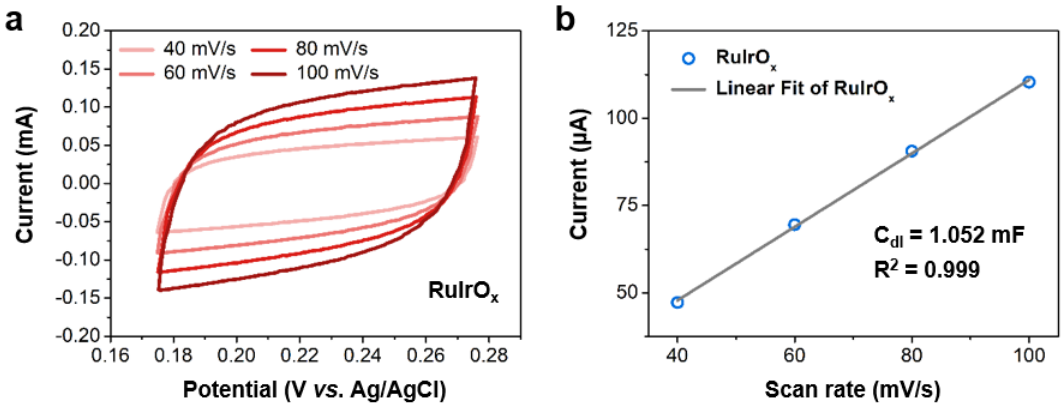

Figure S13. (a) CV curves recorded at different scan rates for $RuIrO_x$ catalyst in a non-Faradaic potential window from 0.175 to 0.275 V (vs. Ag/AgCl). **(b)** Current as a function of scan rate to give the C_{dl} for $RuIrO_x$ catalyst.

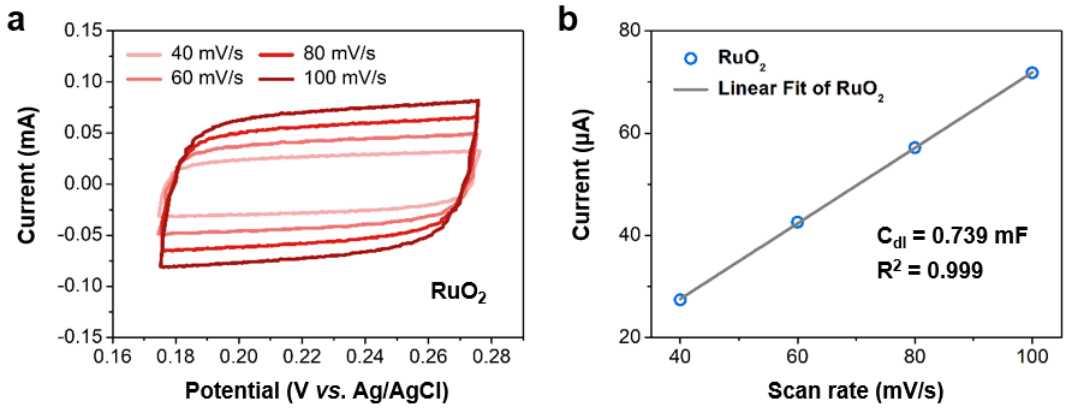

Figure S14. (a) CV curves recorded at different scan rates for RuO_2 catalyst in a non-Faradaic potential window from 0.175 to 0.275 V (vs. Ag/AgCl). **(b)** Current as a function of scan rate to give the C_{dl} for RuO_2 catalyst.

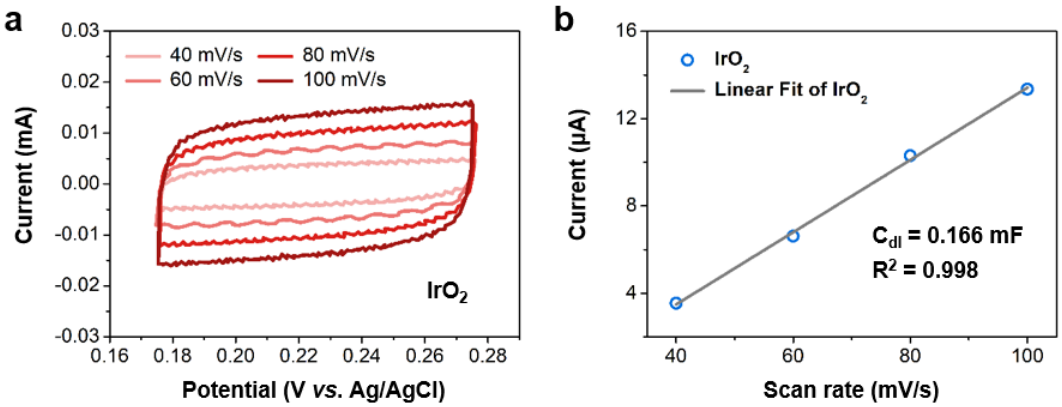

Figure S15. (a) CV curves recorded at different scan rates for IrO_2 catalyst in a non-Faradaic potential window from 0.175 to 0.275 V (vs. Ag/AgCl). **(b)** Current as a function of scan rate to give the C_{dl} for IrO_2 catalyst.

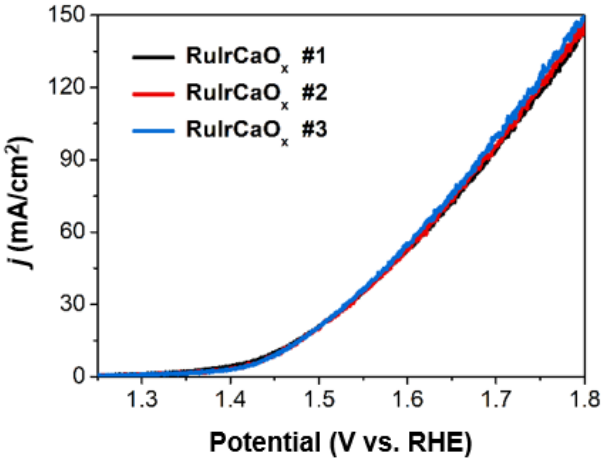

Figure S16. Three independent LSV measurements for $RuIrCaO_x$ catalyst on gold foam electrode obtained at a scan rate of 1 mV/s in CO_2-saturated 0.5 M $KHCO_3$ aqueous electrolyte, respectively.

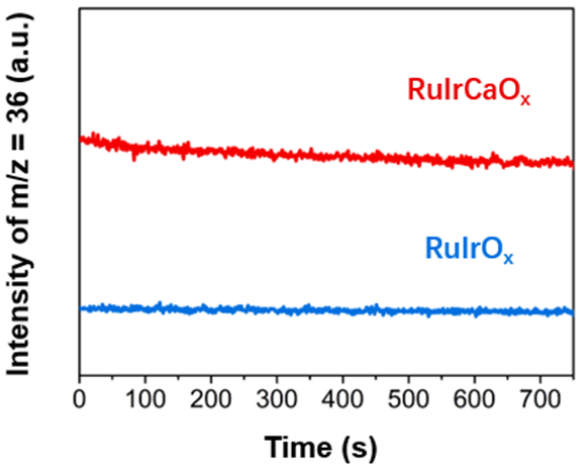

Figure S17. DEMS measurements of the $^{18}O^{18}O$ (m/z=36) signals from the reaction products for ^{18}O-labeled $RuIrCaO_x$ and $RuIrO_x$ catalysts in $H_2{}^{16}O$ aqueous electrolyte.

As shown in Figure S17, no peaks of $^{36}O_2$ ($^{18}O^{18}O$) signals were found for ^{18}O-labeled $RuIrCaO_x$ and $RuIrO_x$ catalysts during the *in-situ* DEMS measurements. These results indicated that it was not found for the reaction pathway where two lattice oxygen atoms coupled with each other and generated $^{36}O_2$ product.

Table S1. Molar ratios of metal elements from ICP-MS for $RuIrCaO_x$ and $RuIrO_x$.

Sample	Element	Molar ratio
$RuIrCaO_x$	Ru	0.49
	Ir	0.24
	Ca	0.43
$RuIrO_x$	Ru	0.50
	Ir	0.21

Table S2. The peak fitting results of O 1s XPS data of $RuIrCaO_x$ and $RuIrO_x$.

Sample	Species	Percentage (%)
$RuIrCaO_x$	Lattice oxygen	34.5
	Adsorbed OH	48.2
	Adsorbed H_2O	17.3
$RuIrO_x$	Lattice oxygen	51.3
	Adsorbed OH	33.4
	Adsorbed H_2O	15.3

Table S3. Parameters for each catalyst investigated on GCEs in CO_2-saturated 0.5 M $KHCO_3$ aqueous electrolyte.

Sample	η^1 (mV)	C_{dl} (mF)	ECSA area (cm^2)	Mass activity (A/g)	Specific activity[2] (mA/cm^2)	TOF[3] (s^{-1})
$RuIrCaO_x$	250	1.163	33.23	93.05	0.084	0.361
$RuIrO_x$	314	1.052	30.06	53.76	0.054	0.174
RuO_2	441	0.739	21.11	15.81	0.023	0.054
IrO_2	665	0.166	4.74	2.52	0.016	0.008

[1] Overpotentials at 10 mA/cm^2, currents are normalized to projected geometric area.

[2] Calculated according to ECSA area. η=400 mV.

[3] Calculated according to the mass loading of active metal atoms. η=400 mV.

Table S4. Summary of the recent reports on OER catalysts in neutral electrolyte.

Sample	pH	On GCE	On Foam	Reference
		η at 10 mA/cm^2 (mV)	**η at 10 mA/cm^2 (mV)**	
$RuIrCaO_x$	**7.2**	**250±4**	**226±4**	**This work**
Co_4Mo	7.2	456		[3]
NiFeCoP	7.2	560	330	[4]
IrO_2	7.1	520[a]		[5]
NiFeMg	7.2	514	310	[6]
$(Fe_xNi_{1-x})_2P$	7.0		396	[7]
CoO/Co_4N	7.0		398	[8]
Co_2P	7.0	592		[9]
Co-Pi	7.0		450[b]	[10]
CoO	7.0	851		[11]
Ni	7.0		600	[12]
IrO_2	7.2		460[c]	[13]

a. FTO glass

b. Ti mesh

c. Ti plate

References for the Supporting Information

[1] B. Zhang, X. L. Zheng, O. Voznyy, R. Comin, M. Bajdich, M. Garcia-Melchor, L. L. Han, J. X. Xu, M. Liu, L. R. Zheng, F. P. G. de Arquer, C. T. Dinh, F. J. Fan, M. J. Yuan, E. Yassitepe, N. Chen, T. Regier, P. F. Liu, Y. H. Li, P. De Luna, A. Janmohamed, H. L. Xin, H. G. Yang, A. Vojvodic, E. H. Sargent, *Science* **2016**, *352*, 333.

[2] Y. T. Kim, P. P. Lopes, S. A. Park, A. Y. Lee, J. Lim, H. Lee, S. Back, Y. Jung, N. Danilovic, V. Stamenkovic, J. Erlebacher, J. Snyder, N. M. Markovic, *Nat. Commun.* **2017**, *8*, 1449.

[3] Y. T. Xu, Z. M. Ye, J. W. Ye, L. M. Cao, R. K. Huang, J. X. Wu, D. D. Zhou, X. F. Zhang, C. T. He, J. P. Zhang, X. M. Chen, *Angew. Chem., Int. Ed.* **2019**, *58*, 139.

[4] X. L. Zheng, B. Zhang, P. De Luna, Y. F. Liang, R. Comin, O. Voznyy, L. Han, F. P. G. de Arquer, M. Liu, T. D. Cao, T. Regier, J. J. Dynes, S. S. He, H. L. L. Xin, H. S. Peng, D. Prendergast, X. W. Du, E. H. Sargent, *Nat. Chem.* **2018**, *10*, 149.

[5] Gurudayal, J. Bullock, D. F. Sranko, C. M. Towle, Y. Lum, M. Hettick, M. C. Scott, A. Javey, J. Ager, *Energy Environ. Sci.* **2017**, *10*, 2222.

[6] N. Wang, Z. Cao, X. L. Zheng, B. Zhang, S. M. Kozlov, P. N. Chen, C. Q. Zou, X. B. Kong, Y. Z. Wen, M. Liu, Y. S. Zhou, C. T. Dinh, L. R. Zheng, H. S. Peng, Y. Zhao, L. Cavallo, X. D. Zhang, E. H. Sargent, *Adv. Mater.* **2020**, 1906806.

[7] B. W. Zhang, Y. H. Lui, H. W. Ni, S. Hu, *Nano Energy* **2017**, *38*, 553.

[8] R. Q. Li, P. F. Hu, M. Miao, Y. L. Li, X. F. Jiang, Q. Wu, Z. Meng, Z. Hu, Y. Bando, X. B. Wang, *J. Mater. Chem. A* **2018**, *6*, 24767.

[9] K. Xu, H. Cheng, L. Liu, H. F. Lv, X. J. Wu, C. Z. Wu, Y. Xie, *Nano Lett.* **2017**, *17*, 578.

[10] L. S. Xie, R. Zhang, L. Cui, D. N. Liu, S. Hao, Y. J. Ma, G. Du, A. M. Asiri, X. P. Sun, *Angew. Chem., Int. Ed.* **2017**, *56*, 1064.

[11] C. W. Tung, Y. Y. Hsu, Y. P. Shen, Y. X. Zheng, T. S. Chan, H. S. Sheu, Y. C. Cheng, H. M. Chen, *Nat. Commun.* **2015**, *6*, 8106.

[12] H. Schaefer, D. M. Chevrier, P. Zhang, J. Stangl, K. Mueller-Buschbaum, J. D. Hardege, K. Kuepper, J. Wollschlaeger, U. Krupp, S. Duehnen, M. Steinhart, L. Walder, S. Sadaf, M. Schmidt, *Adv. Funct. Mater.* **2016**, *26*, 6402.

[13] M. Schreier, L. Curvat, F. Giordano, L. Steier, A. Abate, S. M. Zakeeruddin, J. S. Luo, M. T. Mayer, M. Graetzel, *Nat. Commun.* **2015**, *6*, 7326.